

P. Day · H.G. Leduc · C.D. Dowell · R.A.
Lee · J. Zmuidzinas

Distributed Antenna-coupled TES for FIR detector arrays

06.21.2007

Keywords TES, antenna, FIR

Abstract We describe a new architecture for a superconducting detector for the submillimeter and far-infrared. This detector uses a distributed hot-electron transition edge sensor (TES) to collect the power from a focal-plane-filling slot antenna array. The sensors lay directly across the slots of the antenna and match the antenna impedance of about 30 ohms. Each pixel contains many sensors that are wired in parallel as a single distributed TES, which results in a low impedance that readily matches to a multiplexed SQUID readout. These detectors are inherently polarization sensitive, with very low cross-polarization response, but can also be configured to sum both polarizations. The dual-polarization design can have a bandwidth of 50The use of electron-phonon decoupling eliminates the need for micro-machining, making the focal plane much easier to fabricate than with absorber-coupled, mechanically isolated pixels. We discuss applications of these detectors and a hybridization scheme compatible with arrays of tens of thousands of pixels.

PACS numbers:

1 Introduction

The next generation of astronomical instruments for Submillimeter and FIR wavelengths will require arrays of tens of thousands of pixels. For example, the proposed Caltech-Cornell Atacama Telescope will need 32,000 pixels at 620, 450, 350 and 200 microns to fully sample its field of view. The Single Aperature Far-Infrared Observatory (SAFIR) mission, still a priority of the science community,

Jet Propulsion Laboratory
Pasadena, CA 91109, USA
Tel.:818-354-9356
Fax:818-393-4540
E-mail: Peter.K.Day@jpl.nasa.gov

will require an array with approximately 128×128 detectors with a very high sensitivity of around $10^{-18} \text{W/Hz}^{1/2}$ to be photon noise limited.

When they are fielded, the SCUBA-2 arrays will represent the state-of-the-art in this wavelength range, incorporating thousands of pixels at 850 and 350 microns¹, which is an order of magnitude more than current pioneering instruments such as the Submillimeter High Angular Resolution Camera II (SHARC-II)^{2,3} and Bolocam⁴. Micromachined silicon nitride arrays of TES bolometers along the lines of those used for SCUBA-II could be extended by yet another order of magnitude in pixel count, but would likely be expensive.

A pixel architecture that is both easier to manufacture and compatible with the high sensitivity needed for a space mission would be desirable. In the area of millimeter-wave detectors, detector designs incorporating antenna-coupled TES bolometers have been proposed and demonstrated^{5,6}. In these devices, power from a planar antenna is transmitted down a transmission line to a load resistor, which is thermally isolated on a small island along with a TES. Antenna-coupled pixels have several important advantages. First, only the load resistor and TES need to be thermally isolated, so the micromachined structures are much simpler. Second, the specific heat of the absorber is avoided, so the detectors can be much faster. Third, no backshort is needed as the antenna lies on a substrate with high dielectric constant, so most of the power is radiated into the substrate (hence, most of the power incident on the antenna through the substrate can be efficiently absorbed). The millimeter-wave antenna-coupled devices have additional benefits: phased array antennas can be used that have narrow beam widths that couple easily to a telescope, and filters can be inserted in the microstrip transmission line between antenna and TES to define the pass-band.

For very short wavelengths, microstrip cannot be used to transport power between antenna and detector because because the microstrip becomes lossy at frequencies higher than the gap frequency, about 700 GHz for niobium. Proposed antenna-coupled FIR/Submillimeter detectors therefore collocate the sensor with the antenna^{7,8}. In these cases, the power collected by the antenna is dissipated directly in the TES and the thermal isolation is achieved through the thermal decoupling of the electrons and phonons in the TES, *ie.* the "hot electron" effect. The thermal conductance is then proportional to the volume of the sensor, prescribing a very small TES volume for low enough G . One drawback of the simple hot-electron antenna-coupled detector is that the active area of the antenna is much smaller than the pixel size, which is $kf\lambda$ for a given f /number. For Nyquist sampling, $k = 0.5$. Hence, to efficiently fill the focal plane, an aperture-defining dielectric lens must be placed in front of each antenna.

2 Pixel Design

Our new pixel design⁹ makes use of an array of slot antennas, which is essentially a scaled down version of the microstrip coupled slot array antennas used at millimeter wavelengths. Rather than feeding the slots with microstrips, we directly tap the slot array with an array of TES microbolometers (fig. 1). The microbolometers are made from a thin film of a superconductor with an appropriate T_c with dimensions in the range of one to tens of microns on a side. The normal resistance of the

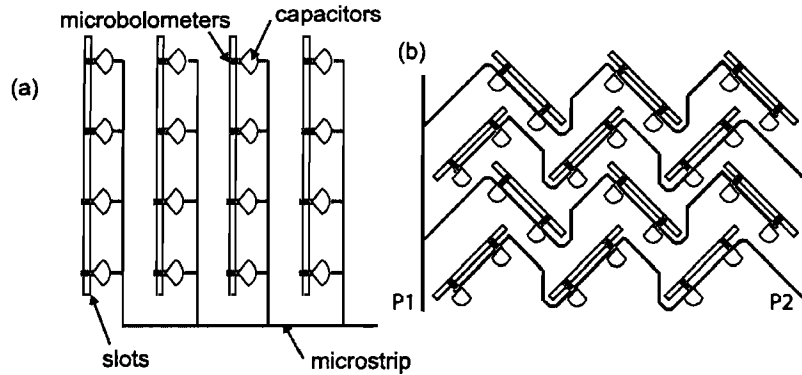


Fig. 1 (a) Design of the (a) single polarization and (b) dual polarization pixels. An array of slots on a ground-plane is tapped directly by an array of microbolometers. Typically arrays of 8×8 or 16×16 microbolometers will be used, depending on the desired pixel size. A reduced number is shown for clarity.

microbolometer is chosen to match to the antenna. A microbolometer is placed at each of the feedpoints where, in the millimeter-wave version of the antenna, a microstrip line would tap the antenna. To allow for biasing of the microbolometers, a DC connection is made between the microbolometer and the ground plane of the slot on one side of the slot. On the other side, the microbolometer is connected through a capacitor large enough to present a short at the frequency of the antenna.

The microbolometers for a particular pixel are all biased in parallel with a bias line that snakes between the slots. The bias line is implemented in microstrip even though it only carries the low frequency output of the bolometer. Use of microstrip in this case conveniently hides the wiring behind the antenna groundplane. The arrangement of slots in fig. 1(b) allows for polarization sensitive imaging as separate bias lines may be used for the different slot directions. For non-polarization sensitive applications, a single bias line may be used.

The parallel bias scheme effectively impedance matches the antenna array and the SQUID amplifier that is used to for the readout of the detector. Each of the microbolometers has a normal state resistance on the order of 30Ω in order to match to the antenna impedance. The impedance seen by the SQUID is the parallel combination of $\sim 64 - 256$ microbolometers, depending on the pixel size (see below). The resulting normal state resistance of the parallel combination, on the order of a few hundred milliohms, allows the use of a bias point in the middle of the transition curve, where low noise operation is typically observed, while maintaining compatibility with current SQUID multiplexers.

As with the millimeter-wave antennas, the slot array pixels are intended to fill a focal plane without the need for lenses or feedhorns. In contrast with the microstrip coupled devices, the detectors we describe here are multimode detectors. Because the radiation collected by the slot array is combined incoherently these antennas do not have a narrow beam pattern, but rather absorb radiation over a broad range of angles similar to a resistive absorber. These detector arrays are

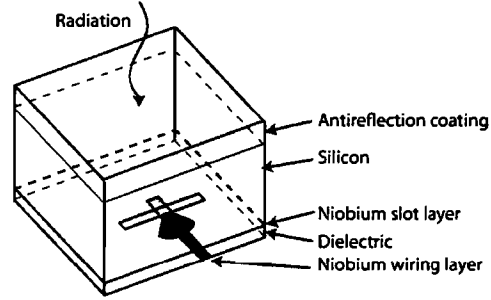


Fig. 2 The antennas are illuminated through the back of the silicon wafer on which they are fabricated. Because the substrate has a high dielectric constant, the antenna efficiently absorbs radiation in this direction. An antireflection coating matches to free space or a resonant ($\lambda/4$) substrate may be used.

therefore comparable to the arrays of bare absorbers used for SHARC-II^{2,3} and SCUBA-II¹.

Just as with the single-moded microstrip-coupled antennas, the slot spacing, δ_s , should satisfy $\delta_s < \lambda/\sqrt{\epsilon_r}$, where ϵ_r is the relative dielectric constant of the substrate, to avoid coupling to substrate modes⁶. For the single mode devices, coupling to substrate modes reduces the efficiency of the detector. In the case of the multimode detectors, the incoming wave drives the slots coherently, so satisfying the criterion on δ_s will prevent the scattered wave from the antenna from coupling into substrate modes, which would be a source of cross-talk. For $f/4$ and a silicon substrate ($\epsilon_r = 11.5$), the number of microbolometers is approximately 64 for $0.5f\lambda$ pixels (Nyquist sampling) and 256 for $f\lambda$ pixels.

The thermal noise is

$$\text{NEP}_{\text{thermal}} = \sqrt{4k_B T^2 G}, \quad (1)$$

where G is the combined thermal conductance between electrons and phonons for all of the microbolometers in a pixel and is proportional to the total volume.

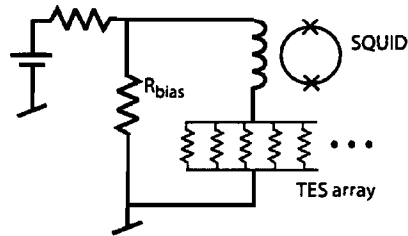


Fig. 3 The array of microbolometers corresponding to a particular pixel are biased in parallel. This scheme effectively matches the antenna impedance of $\sim 30\Omega$ to the SQUID multiplexer, which requires a TES resistance of less than an ohm.

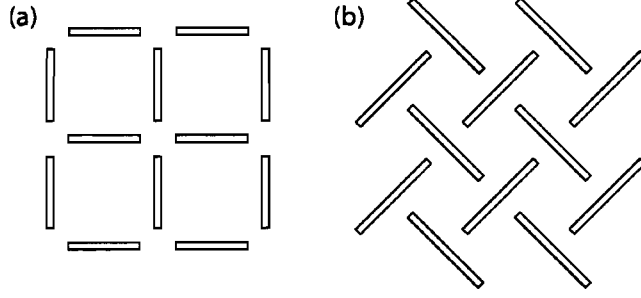


Fig. 4 (a) Geometry of the 'L' antenna. (b) The new 'H' geometry allows the slots to be longer relative the spacing between them, improving the bandwidth

Hence, the NEP of an individual microbolometer would be \sqrt{N} times smaller than the combination if it were biased separately.

3 Antenna Design

The antennas described here are essentially scaled down versions of the millimeter-wave microstrip-coupled slot arrays^{6,10}. The incoherently combined FIR detectors will have broad beam patterns relative to the coherently combined slot arrays, but the impedance of the antennas will be similar. For example, if we illuminate the incoherent slot arrays with the same beam generated by the coherent antenna ($\sim f/4.5$), by reciprocity the voltage across the individual slots must be identical in either case. Hence we can use the same method to calculate the antenna impedance.

Here we describe a new wider-bandwidth version of the dual polarization slot array antenna that can be used for both FIR and millimeter wave focal planes. The old and new geometries, which we will refer to as the 'L' and 'H' geometries, respectively, are depicted in fig. 4. The 'H' geometry can be generated from the 'L' geometry by rotating all of the slots by 45 degrees and lengthening them. The main difference with the new design is that the slots can be made longer relative to the lattice spacing while maintaining the same gap between slots.

The impedance of the antennas is calculated using the same method-of-moments procedure used for microstrip-coupled slot antennas^{11,12} and slot arrays¹⁰. In this method, the electric field in the slots is expanded in terms of a set of appropriate basis functions,

$$E_{\alpha}(x,y) = \sum_i V_{\alpha,i} f_{\alpha,i}(x,y), \quad (2)$$

where $\alpha = \{x,y\}$ and we make the approximation that $E_x = 0$ for \hat{x} -directed slots and $E_y = 0$ for \hat{y} -directed slots. The admittance kernel

$$Q_{\alpha\beta}(k_x, k_y) = \frac{1}{Z_0} \left[\left(\frac{\epsilon_1 k}{\gamma_1} + \frac{\epsilon_2 k}{\gamma_2} \right) \delta_{\alpha\beta} - \left(\frac{1}{k\gamma_1} + \frac{1}{k\gamma_2} \right) p_{\alpha} p_{\beta} \right], \quad (3)$$

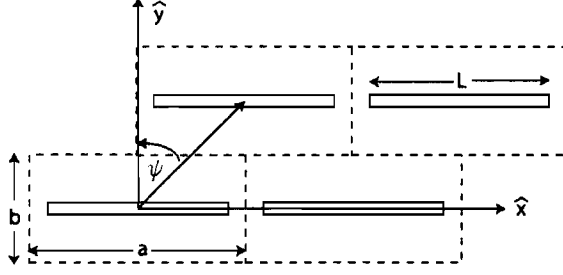


Fig. 5 Skewed lattice corresponding to the infinite array case of the new dual-polarization antenna. Only one slot direction is shown.

where $\delta_{\alpha\beta}$ is the Kronecker delta function, $\alpha, \beta = x$ or y , $\vec{p} = (k_y, k_x, 0)$, $\epsilon_{1,2}$ are the dielectric constants above and below the antenna plane, $\gamma_i^2 = \epsilon_i k^2 - k_x^2 - k_y^2$ ($Im\{\gamma_1\} \leq 0$, $Im\{\gamma_2\} \geq 0$), and Z_0 is the impedance of free space.

Using the Galerkin method, a matrix equation is written for the unknown basis function amplitudes in terms of the currents in the slots:

$$I_i = \sum_j Y_{ij} V_j, \quad (4)$$

where \vec{T} is the vector of overlap integrals between the slot currents and the basis functions and

$$Y_{ij} = \frac{-1}{4\pi^2} \int_{-\infty}^{\infty} \int_{-\infty}^{\infty} dk_x dk_y Q_{\alpha\beta}(k_x, k_y) \tilde{f}_i^*(k_x, k_y) \tilde{f}_j(k_x, k_y), \quad (5)$$

where \tilde{f}_i are the Fourier transforms of the basis functions, and the proper form of $Q_{\alpha\beta}$ is used depending on whether basis functions i and j belong to parallel or perpendicularly oriented slots. Once the basis function amplitudes are evaluated, the impedance at the feed points is determined from the ratio of the voltage to the current at those points.

In the case of an infinite array of slots, only wave vectors that reflect the periodicity of the lattice are allowed and the integrals are replaced by sums. For the 'H' antenna, it is convenient to use a skewed lattice and slots oriented in the \hat{x} direction (fig. 5). In this case, the wave vectors satisfy¹³

$$k_{x,mn} = \frac{2m\pi}{a} \quad (6)$$

$$k_{y,mn} = \frac{2n\pi}{b} - \frac{2m\pi}{b} \tan \psi, \quad (7)$$

where $\psi = \pi/4$. The admittance matrix becomes

$$Y_{ij} = \frac{-1}{ab} \sum_{mn} Q_{\alpha\beta}(k_{x,mn}, k_{y,mn}) \tilde{f}_i^*(k_{x,mn}, k_{y,mn}) \tilde{f}_j(k_{x,mn}, k_{y,mn}), \quad (8)$$

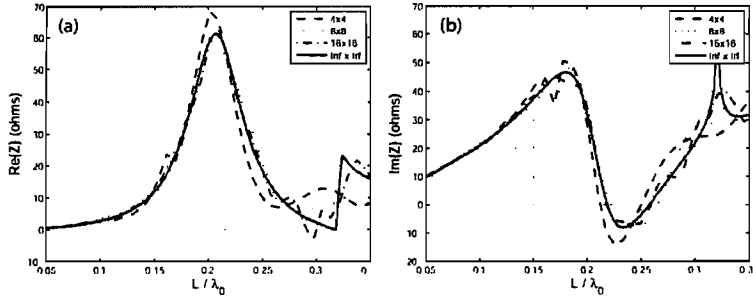


Fig. 6 (a) Real and (b) imaginary parts of the impedance of the 'H' antenna versus L/λ_0 , where L is the length of the slot and λ_0 is the free space wavelength, for 4×4 , 8×8 , 16×16 elements and infinite arrays. The lattice spacing is $1.3L$, $W = 0.04$ and the feed points are $\pm 0.38L$.

where m, n are integers.

The method-of-moments calculations were performed using 11 piecewise sinusoidal basis functions per slot¹¹. Increasing the number of basis functions produced essentially the same results. We have calculated both the infinite array and finite arrays of various numbers of elements up to 16×16 . As shown in fig. 6, the impedance of the 16×16 array is very close to that of the infinite array.

We operate the antenna near the peak due to the first resonance in order to stay well below the frequency where grating lobes become an issue. For a feed point centered in the slot, the impedance at the peak is $\sim 150\Omega$. Operating with such a large microbolometer resistance would be possible, but would lead to a parallel resistance that is still somewhat high for the SQUID readout. (For the millimeter wave version of the antenna, it would be difficult to make the impedance of the mi-

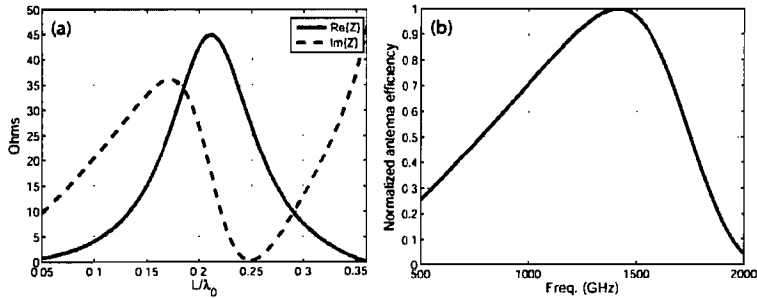


Fig. 7 (a) Impedance of the dual polarization antenna. The substrate is silicon ($\epsilon = 11.5$) and the width of the slot is $0.04L$. The feed points are located at $\pm 0.38L$, and the lattice spacing is $1.1L$. (b) Normalized efficiency of the antenna with 28Ω microbolometers. The length of the slot is chosen to center the pass band at 1.4 THz. The bandwidth is large enough to cover the 1.3 and 1.5 THz atmospheric windows with 90% efficiency.

crostrip line this large.) In order to reduce the impedance of the antenna we move the feed points toward the end of the slots. We use two feeds per slot in order to maintain symmetry (fig. 1(b)) which results in very low cross polarization. In the case of the infinite array, the cross-polarization coupling vanishes. For finite arrays, coupling between nearest neighbor slots of differing polarizations vanishes, so the only cross-polarization coupling can be from more distant neighbors around the edges of the array where the symmetry is broken.

Feeding the slots near the ends makes the antenna more inductive, so that the imaginary part of the impedance no longer goes to zero at the peak in the real part, as is the case for a center-fed slot. A purely real impedance is obtained by operating on the high frequency side of the peak (fig. 7), which results in a somewhat asymmetric pass band and a bandwidth $\delta f(3dB)/f_{center} = 0.77$ (for a lattice constant of $1.1L$).

4 Conclusions

We have described a new pixel design that is applicable to large focal plane arrays for submillimeter and FIR wavelengths. An improved version of the dual polarization slot array antenna has been designed that increases the bandwidth over an earlier design⁹. Arrays of dual-polarization antenna-coupled detectors bring several practical benefits to astronomical instruments in the field. Maximum sensitivity is achieved over the detector field of view, which is important for many imaging applications. Common mode signals such as atmospheric emission and thermal drift of the focal plane are rejected optimally in the measurement of polarization since each diffraction beam is observed in both polarizations and since the distributed TES arrays should be electrically well matched for each polarization. The monolithic approach significantly reduces complexity as compared to separate arrays observing orthogonal polarizations, ortho-mode transducers, or stacked polarization-sensitive detectors.

References

1. W. Duncan et al. SCUBA-2: Application of LTD technology. *AIP Conference Proceedings, LTD-9*, 605:577–580, 2002.
2. G. M. Voellmer, C. A. Allen, M. J. Amato, S. R. Babu, A. E. Bartels, D. J. Benford, R. J. Derro, C. D. Dowell, D. A. Harper, M. D. Jhabvala, S. H. Moseley, T. Rennick, P. J. Shirron, and J. G. Staguhn. Design and fabrication of two-dimensional semiconducting bolometer arrays for the high-resolution airborne wideband camera (HAWC) and the submillimeter high angular resolution camera II (SHARC-II). *Proc. SPIE*, 4855:63–72, 2002.
3. C. D. Dowell, C. A. Allen, S. R. Babu, M. M. Freund, M. B. Gardner, J. Groseth, M. D. Jhabvala, A. Kovacs, D. C. Lis, S. H. Moseley, T. G. Phillips, Silverberg R. F., G. M. Voellmer, and H. Yoshida. Sharc-II: A caltech submillimeter observatory facility camera with 384 pixels. *Proc. SPIE*, 4855:73–87, 2002.
4. J. Glenn, J. J. Bock, G. Chattopadhyay, S. F. Edgington, A. E. Lange, J. Zmuidzinas, P. D. Maukopf, B. Rownd, L. Yuen, and P. A. R. Ade. Bolocam: a millimeter-wave bolometric camera. *Proc. SPIE*, 3354:326–334, May 2002.
5. C. L. Hunt, J. J. Bock, P. K. Day, A. Goldin, A. E. Lange, H. LeDuc, A. Vayonakis, and J. Zmuidzinas. Transition-edge superconducting antenna-coupled bolometer. *Proc. SPIE*, 3354:318–321, May 2002.
6. A. Goldin, J. J. Bock, C. Hunt, A. E. Lange, H. LeDuc, A. Vayonakis, and J. Zmuidzinas. Design of broadband filters and antennas for SAMBA. *Proc. SPIE*, 3354:163–171, May 2002.
7. M. Nahum and J. M. Martinis. Ultrasensitive-hot-electron microbolometer. *Appl. Phys. Lett.*, 63(22):3075–3077, Nov 1993.
8. B. S. Karasik, W. R. McGrath, M. E. Gershenson, and A. V. Sergeev. Photon-noise-limited direct detector based on disorder-controlled electron heating. *J. Appl. Phys.*, 87(10):7586–7588, May 2000.
9. P. K. Day, H. LeDuc, A. Goldin, C.D. Dowell, and J. Zmuidzinas. *Proc. SPIE*, 5498:857–865, 2002.
10. A. Goldin, J. J. Bock, A. E. Lange, H. LeDuc, A. Vayonakis, and J. Zmuidzinas. Antennas for bolometric focal plane. *Nuclear Instruments and Methods in Physics Research Section A*, 520:390–392, 2004.
11. M. Kominami, D. Pozar, and D. Schaubert. Dipole and slot elements and arrays on semi-infinite substrates. *AP*, 33(6):600–607, 1985.
12. J. Zmuidzinas and H. G. LeDuc. Quasi-optical slot antenna SIS mixers. *IEEE Trans. Microwave Theory Tech.*, MTT-40:1797–1804, 1992.
13. Craig Scott. *The Spectral Domain Method in Electromagnetics*. Artech House, Inc.: Norwood, MA, 1998.

Distributed Antenna-Coupled TES for FIR Detector Arrays

Peter Day, Rick Leduc, Darren Dowell
Jet Propulsion Laboratory

Jonas Zmuidzinas, Richard Lee
California Institute of Technology



We describe a new architecture for a superconducting detector for the submillimeter and far-infrared. This detector uses a distributed hot-electron transition edge sensor (TES) to collect the power from a focal-plane-filling slot antenna array. The sensors lay directly across the slots of the antenna and match the antenna impedance of about 30 ohms. Each pixel contains many sensors that are wired in parallel as a single distributed TES, which results in a low impedance that readily matches to a multiplexed SQUID readout. These detectors are inherently polarization sensitive, with very low cross-polarization response, but can

also be configured to sum both polarizations. The dual-polarization design can have a bandwidth of 50% and a quantum efficiency greater than 90% when used with a quarter-wavelength substrate. The use of electron-phonon decoupling eliminates the need for micro-machining, making the focal plane much easier to fabricate than with absorber-coupled, mechanically isolated pixels. We discuss applications of these detectors and a hybridization scheme compatible with arrays of tens of thousands of pixels.

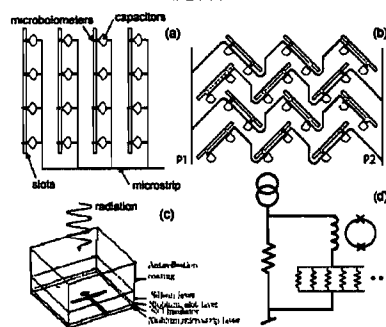
Introduction

- Antenna-coupled pixels are an attractive option for detection of mm - FIR wavelengths. For mm-waves antenna coupling using a microstrip line has been demonstrated^{1,2,3}.
- For frequencies > ~700 GHz (gap frequency of niobium), the superconducting transmission lines become lossy and can no longer transmit power over the required distances ~ λ .
- For FIR/Submm detectors, antenna-coupled designs have been proposed with the sensor collocated with the antenna^{4,5}, where the power collected by the antenna dissipates directly in the TES. The normal resistance of the TES must be matched to the antenna impedance for efficient absorption, but that relatively large impedance may be difficult to match with multiplexed SQUID readouts.
- Here we describe a new pixel architecture based on a parallel biased distributed array of microbolometers.

Pixel Architecture

- An array of slots in a ground plane is periodically tapped directly by an array of TES hot-electron microbolometers (fig. 1a)
- Single (all slots parallel) or Dual (interspersed perpendicular slots) polarization configurations are possible.
- Slot spacing, δ_s , satisfies $\delta_s < \lambda / \epsilon_r^{1/2}$ to preclude scattering into surface waves.
- The number of slots/ microbolometers can be tailored to produce $\frac{1}{2} F\lambda$ or $F\lambda$ pixels (approximately 64 and 256, respectively.)
- The microbolometers for a pixel are biased in parallel (fig. 1d).
- The power absorbed by the microbolometers combines incoherently, so the detector is multimode.
- For ~30 ohms per microbolometer (matching the antenna), the parallel combination is ~ 100 to 400 m Ω , depending on the number of microbolometers per pixel.

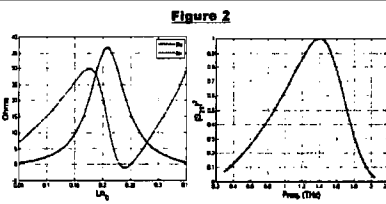
Figure 1



Layout of single (a) and dual (b) pol antennas. A reduced number of elements is shown for clarity. (c) The antennas are illuminated through the back of a silicon wafer. (d) Parallel bias of the bolometers for a particular pixel.

- The distributed design fills the focal plane area without the need for lenses.

Efficiency



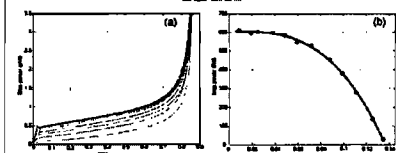
Method of moments⁶ calculation of the dual-pol antenna impedance (slot length chosen for operation at 1.4THz.)

- Bandwidth ~50% for the dual pol detector. The single pol antenna can be very wide band ~10:1

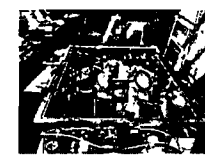
- Power "radiated" by the antenna is directed into the substrate. The power division ratio is approximately $\epsilon_r^{1/2}$:1, giving an efficiency of about 71% for a silicon substrate.
- A $1/4$ - λ resonant substrate can be used, in which case the power division ratio is ϵ_r :1 (about 90% efficiency).

Measurements

Figure 3



Bias curves for a parallel combination of 64 microbolometers, each 1 μ m on a side, made from a 20nm thick titanium film with a transition temperature of 140mK. $G = 14$ pW/K @140mK. At 100mK the phonon NEP for this device is 2×10^{-16} W/Hz^{1/2}.



A vacuum FTS (Martin-Puplett Spectrometer) has been assembled for measuring detector spectral response.



Radiation from the spectrometer shines into a dilution refrigerator.

References

1. C. L. Hunt et al., Proc. SPIE, 3354:316-321, May 2002.
2. A. Golkin et al., Proc. SPIE, 3354:163-171, May 2002.
3. Myers et al. Appl. Phys. Lett. 88, 114103 (2005).
4. Mees et al. Appl. Phys. Lett. 89 (18), pp. 2329
5. M. Nahum et al., Appl. Phys. Lett., 63(22):3075-3077, Nov 1993
6. S. S. Karsak et al., J. Appl. Phys., 87(10) 7586-7588, May 2000.
7. S. Ali et al., IEEE Trans. Applied Superconductivity, 13(2):164-167, 2003.